



3-(benzo[d]thiazol-2-YL)phenol and 4-(benzo[d]thiazol-2-YL)phenol: Crystal Structure Determination, DFT Calculations and Visualizing Intermolecular Interactions Using Hirshfeld Surface Analysis

R. K. Mudsainiyan & A. K. Jassal

To cite this article: R. K. Mudsainiyan & A. K. Jassal (2016) 3-(benzo[d]thiazol-2-YL)phenol and 4-(benzo[d]thiazol-2-YL)phenol: Crystal Structure Determination, DFT Calculations and Visualizing Intermolecular Interactions Using Hirshfeld Surface Analysis, Molecular Crystals and Liquid Crystals, 629:1, 120-134, DOI: [10.1080/15421406.2015.1107812](https://doi.org/10.1080/15421406.2015.1107812)

To link to this article: <http://dx.doi.org/10.1080/15421406.2015.1107812>



View supplementary material [↗](#)



Published online: 16 Jun 2016.



Submit your article to this journal [↗](#)



Article views: 38



View related articles [↗](#)



View Crossmark data [↗](#)

3-(benzo[d]thiazol-2-YL)phenol and 4-(benzo[d]thiazol-2-YL)phenol: Crystal structure determination, DFT calculations and visualizing intermolecular interactions using Hirshfeld surface analysis

R. K. Mudsainiyan and A. K. Jassal

Department of Chemistry, Centre for Advanced Studies-I, Guru Nanak Dev University, Amritsar, India

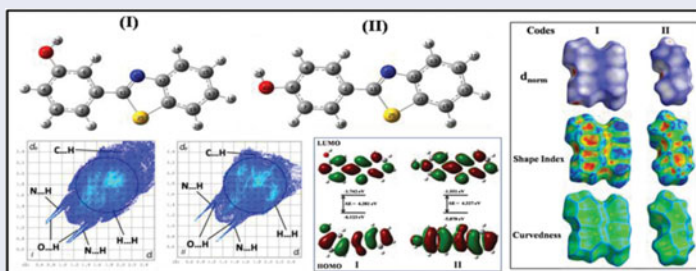
ABSTRACT

This article describes the synthesis and X-ray crystal structure analysis of **3-(benzo[d]thiazol-2-yl) phenol (I)** and **4-(benzo[d]thiazol-2-yl)phenol (II)**, crystallized in centrosymmetric triclinic and orthorhombic space groups respectively. The packing in the unit cell of these two positional isomers are different resulting difference in various types of intermolecular interactions (C-H...S, O-H...O_w and O-H...N) connect the molecules into 2D frameworks. Due to presence of lattice water in compound (I), H-bonding interactions are strong and melting point of (I) is comparatively higher than (II). The DFT optimized molecular geometries in (I) and (II) agree closely with those obtained from crystallographic studies.

KEYWORDS

Centrosymmetric;
2D-fingerprint plot; hirshfeld surface; positional isomers; space group; two-dimensional framework


GRAPHICAL ABSTRACT



The compounds (I) and (II) have been crystallized in centrosymmetric space groups. The DFT optimized molecular geometries in both compounds agree closely with those obtained from the crystallographic studies. An interplay of O-H...O_w and O-H...N type strong hydrogen bonds and C-H...S type weak interactions connect the molecules of (I) and (II) into 2D framework. Hirshfeld surface analysis of (I) indicates that the H...H and H... π contacts can account for 47.4% and 18.7%, respectively, of the Hirshfeld surface area, whereas the corresponding fraction in (II) is 36.5% and 29.5%, respectively.

CONTACT R. K. Mudsainiyan  mudsainiyanrk@gmail.com

Color versions of one or more of the figures in the article can be found online at www.tandfonline.com/gmcl.

 Supplemental data for this article can be accessed at <http://dx.doi.org/10.1080/15421406.2015.1107812>.

© 2016 Taylor & Francis Group, LLC

1. Introduction

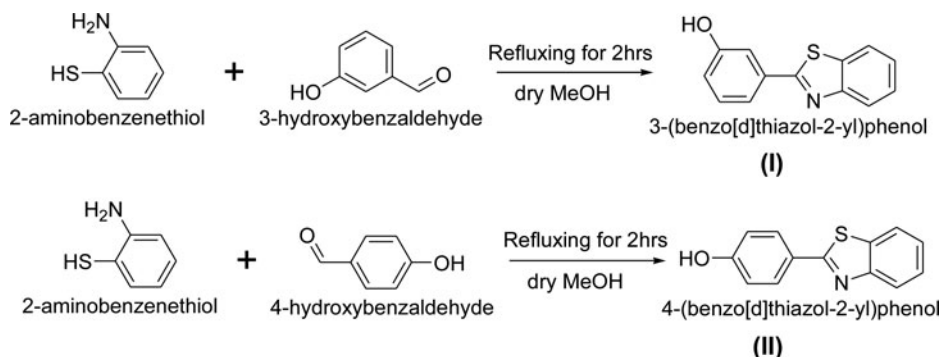
In the past decades, various sulfur and nitrogen-containing heterocyclic compounds and their derivatives have been occurring predominately in nature appreciable to their stability and ease of generating new compounds [1–8]. These compounds exhibit pronounced biological activities, fluorescence properties, various applications in organic electroluminescent devices, biosensors, detection of metal ions, etc. [9–16]. Intermolecular interactions due to particular hydrogen bonds are key factors for the construction of molecular assemblies of neutral organic molecules with donor and acceptor functionalities [17]. Many of the synthons observed in supramolecular chemistry involve strong hydrogen bonds, which provide the requisite robustness and reproducibility to create a variety of solid-state architectures described as layers, rods, tapes, ribbons, channels, helices, and sheets [18]. The intermolecular hydrogen bonding interactions can help to stabilize crystal packing in the unit cell of each system. In addition to these relatively strong hydrogen bonds like O-H ...O_w and O-H ...N, weak hydrogen bonding interactions such as C-H ...S are also important in the description of self-assembly process. The influence of these weak interactions can be evaluated by comparing their structural features as well as the interplay of hydrogen bonds in building possible supramolecular aggregation in closely related compounds. Single-crystal X-ray diffractometry is the method of choice for determination of crystal structure of molecular compounds but an intrinsic limitation of this approach is the requirement to grow single crystals of appropriate size and good quality that make them amenable to structure analysis.

A comparison of the torsion angles between mean planes of the benzene and thiol rings in the crystals with the DFT theoretical calculations have also been performed. The inclusion of weak intermolecular hydrogen bonding interactions from crystallographic data compared with Hirshfeld surface analysis for both compounds. Hirshfeld surface analysis has been used to visualize the molecular shapes employing 3D molecular surface contours and 2D fingerprint plots. Molecular orbital diagrams provide visual representations of the top level molecular orbital surfaces in each compound. This idea prompted us to investigate the structural features of benzothiazole derivatives using X-ray powder diffraction and to analyze the role of O-H ...O_w and O-H ...N hydrogen bonds in building possible supramolecular architecture. The compound (II) is already solved in same space group [19] but we tried to solve it in better way and detail of crystal structure is given along with comparison of two positional isomers (I) and (II). The results of crystal structural study of compounds (I) and (II) are reported here along with the DFT calculations to study the molecular geometry. The intermolecular interactions and their percentage in each compound can be obtained by using Crystal Explorer 3.1 [20].

2. Experimental

2.1. Synthesis of 3-(benzo[d]thiazol-2-yl)phenol (I) and 4-(benzo[d]thiazol-2-yl)phenol (II) (Scheme 1)

2-aminobenzenethiol (0.125g, 1 mmol) was dissolved in dry methanol (10 mL). 3-hydroxybenzaldehyde for (I) and 4-hydroxybenzaldehyde for (II) were dissolved in dry methanol (10 mL) separately. Both solutions of 2-aminobenzenethiol and hydroxybenzaldehyde were mixed slowly and refluxed for 2 h in a round-bottomed flask. The completion of reaction was monitored by TLC. After refluxing, filtered the solution mixture and transferred



Scheme 1. Synthesis of 3-(benzo[d]thiazol-2-yl)phenol (**I**) and 4-(benzo[d]thiazol-2-yl)phenol (**II**)

to a 25mL conical flask for slow evaporation at room temperature. Yellowish crystals were separated out by filtration and dried well.

Compound (**I**), M.p. 183 °C. Anal. Calcd for $C_{26}H_{20}N_2O_3S_2$ (**I**) (%): C, 66.08; H, 4.27; N, 5.93; S, 13.57; Found: C, 66.06; H, 4.29; N, 5.91; S, 13.52. MS (DMSO): m/z 548.06 $[M+DMSO-2]^+$, 476.05 $[M-3]^+$. IR (cm^{-1}) selected bonds: $\nu(-OH) = 3738$ b, $\nu(C-H_{aromatic}) = 3045$ w, $\nu(C=N) = 1654$ w, $\nu(C=C) = 1595$ sh, $\nu(C-S) = 793$ sh.

Compound (**II**), M.p. 176 °C. Anal. Calcd for $C_{13}H_9NOS$ (**II**) (%): C, 68.70; H, 3.99; N, 6.16; S, 14.11; Found: C, 68.76; H, 3.97; N, 6.14; S, 14.12. MS (DMSO): m/z , 227.12 $[M^+, 100\%]$, 228.12 $[M+1]^+$ ion, 229.12 $[M+2]^+$ ion, 226.10 $[M-1]^+$ ion. IR (cm^{-1}) selected bonds: $\nu(-OH) = 3657$ b, $\nu(C-H_{aromatic}) = 2930$ w, $\nu(C=N) = 1620$ w, $\nu(C=C) = 1576$ sh, $\nu(C-S) = 711$ sh. (b = broad, sh = sharp, w = weak).

2.2. Physical measurements

All the starting reagents of analytical grade were used without further purification. C, H, N elemental analyses were obtained with a CHNS-O analyzer flesh-EA-1112 series. The IR spectra of compounds (**I**) and (**II**) were recorded on Perkin ELMER FTIR spectrometer in the range $4000-400\text{ cm}^{-1}$. Single crystal structural X-ray diffraction was carried out on a Bruker's Apex-II CCD diffractometer using Mo $K\alpha$ ($\lambda = 0.71069$) at room temperature. Molecular Hirshfeld surfaces calculations of compounds (**I**) and (**II**) were performed by using the Crystal Explorer 3.1. The 3D d_{norm} surfaces are mapped over a fixed color scale of -1.25 (red) to 1.52 \AA (blue), Shape index mapped in the color range of -1.0 to 1.0 \AA and Curvedness in the range of -4.0 to 0.4 \AA . The 2D fingerprint plots displayed by using the standard $0.58-2.7\text{ \AA}$ view, with the d_e and d_i distance scales displayed on the graph axes. DFT calculations were performed by using Gaussian 03 (G03) and optimized structures were visualized by gauss view. Mass spectra of compounds were recorded on Bruker compass microTOF-Q11.

2.3. X-ray crystallography

The crystals of compounds (**I**) and (**II**) were grown by slow evaporation in dry methanol. X-ray data of both the compounds were collected on a Bruker's Apex-II CCD diffractometer using Mo $K\alpha$ ($\lambda = 0.71069$) at room temperature. The data were corrected for Lorentz and polarization effects and empirical absorption corrections were applied using SADABS from Bruker. A total of 13875 reflections were measured out of which 3964 were independent

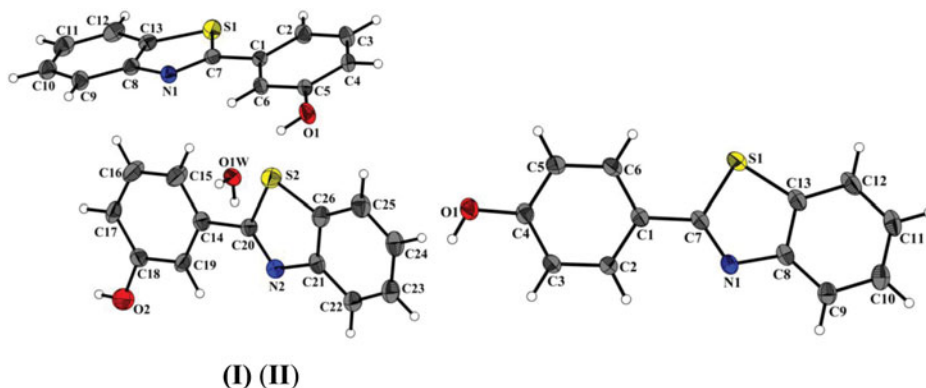


Figure 1. ORTEP showing molecular structures of compounds (I) and (II) (with 20% probability).

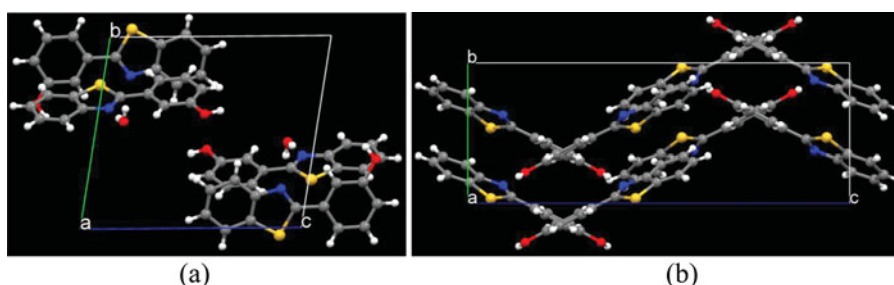


Figure 2. Showing packing diagrams within unit cells of compounds (I) and (II).

for compound (I) and 13856 reflections were measured out of which 3393 were independent for compound (II). The structures of (I) and (II) were solved by direct methods in triclinic P-1 and orthorhombic Pbca space groups, respectively, using SIR-92 [21] and refined by full-matrix least squares refinement methods [22] based on F^2 , using SHELX-97. The protons of the -OH groups of both compounds and lattice water molecule of compound (I) were located from the difference Fourier synthesis and were refined isotropically with U_{iso} values 1.2 times that of their carrier oxygen atoms. All non-hydrogen atoms were refined anisotropically. All hydrogen atoms were fixed geometrically with their U_{iso} values 1.2 times of the phenylene carbons. Geometry of this complex and hydrogen bonding interactions were calculated using

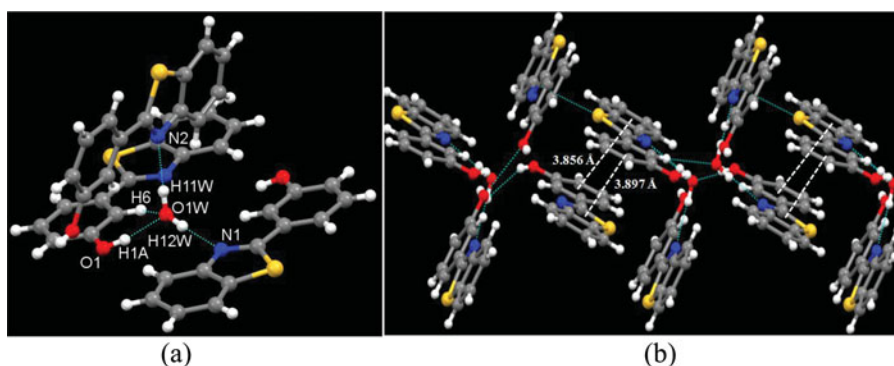


Figure 3. (a) Showing tetrahedral geometry around lattice water in compound (I) along b axis, (b) π - π interactions between phenyl rings, phenyl and thiol rings in ab plane [centroid (C1-C6) ... centroid (C8-C13) = 3.856 Å, centroid (C7-N1-C8-C13-S1) ... centroid (C1-C6) = 3.897 Å].

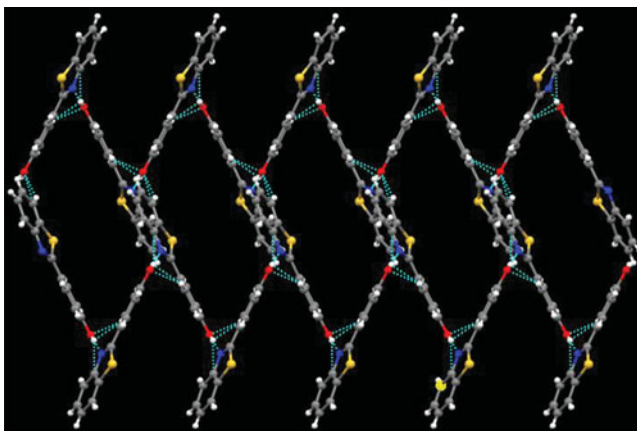


Figure 4. H-bonded network of compound (II) in *bc* plane. π - π interactions are missing but weak CH- π interactions are observed in this compound.

PARST programme [23]. All the drawings of complexes were made using ORTEP [24] and MERCURY [25] programs. All calculations were performed using Wingx package [26]. Structure refinement data of compounds (I) and (II) are given in Table 1 and important H-bonding interactions are shown in Table 2.

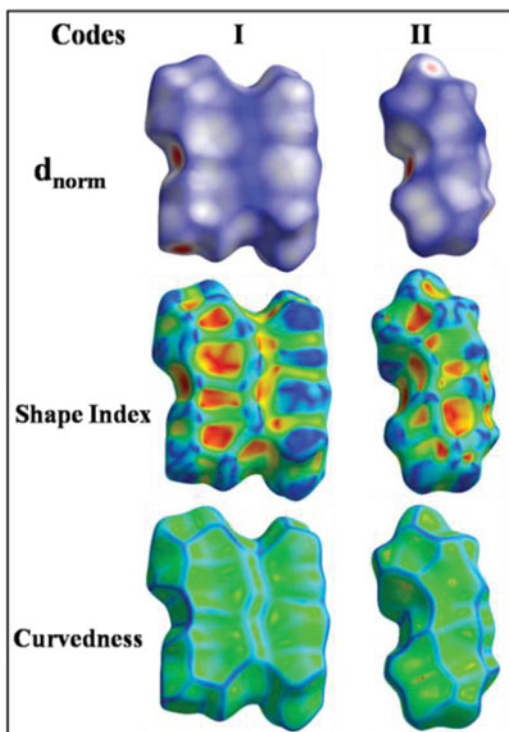


Figure 5. Molecular Hirshfeld d_{norm} surfaces, *shape index* and *curvedness* of compounds (I) and (II), where d_e Surfaces have been mapped between d_e 0.58 and 2.7 Å.

Table 1. Crystal data and structure refinement for compounds (I) and (II).

Identification code	(I)	(II)
Empirical formula	C ₂₆ H ₂₀ N ₂ O ₃ S ₂	C ₁₃ H ₉ NOS
Formula weight	472.58	227.28
Temperature	296(2) K	296(2) K
Wavelength	0.71073 Å	0.71073 Å
Crystal system	Triclinic	Orthorhombic
Space group	P-1	Pbca
Unit cell dimensions	a = 9.9805(11) Å, α = 79.538(5)°. b = 10.0635(11) Å, β = 74.446(6)°. c = 11.9526(13) Å, γ = 84.944(6)°.	a = 13.1739(8) Å, α = 90°. b = 7.7435(5) Å, β = 90°. c = 21.1763(11) Å, γ = 90°.
Volume	1136.3(2) Å ³	2160.2(2) Å ³
Z	2	8
Density (calculated)	1.381 Mg/m ³	1.398 Mg/m ³
Absorption coefficient	0.266 mm ⁻¹	0.274 mm ⁻¹
F(000)	492	944
Crystal size	0.16 × 0.12 × 0.08 mm ³	0.11 × 0.08 × 0.06 mm ³
Theta range for data collection	1.79 to 25.04°.	1.92 to 30.97°.
Index ranges	−11 < = h < = 11, −11 < = k < = 10, −14 < = l < = 14	−18 < = h < = 18, −9 < = k < = 11, −30 < = l < = 25
Reflections collected	13875	13856
Independent reflections	3964 [R(int) = 0.0371]	3393 [R(int) = 0.0271]
Completeness to theta = 25.04°	99.1%	98.8%
Absorption correction	Semi-empirical from equivalents	Semi-empirical from equivalents
Max. and min. transmission	0.7452 and 0.6603	0.7461 and 0.6650
Refinement method	Full-matrix least-squares on F ²	Full-matrix least-squares on F ²
Data / restraints / parameters	3964 / 4 / 310	3393 / 1 / 148
Goodness-of-fit on F ²	1.042	0.954
Final R indices [I > 2sigma(I)]	R1 = 0.0566, wR2 = 0.1539	R1 = 0.0470, wR2 = 0.1337
R indices (all data)	R1 = 0.0890, wR2 = 0.1738	R1 = 0.0909, wR2 = 0.1650
Largest diff. peak and hole	1.142 and −0.369 e. Å ⁻³	0.350 and −0.324 e. Å ⁻³
CCDC number	1034985	1034986

Table 2. Showing important H-bonding interactions in compounds (I) and (II).

Compound (I)	X...Y	Y...H	X-H...Y
X-H...Y			
C2-H2 ...S1	3.088(4)	2.68	108
C6-H6 ...O1W	3.267(4)	2.65	124
C15-H15 ...S2	3.099(5)	2.68	108
O1-H1A ...O1W	2.597(3)	1.78(3)	169
C9-H9 ...O1W ¹	3.547(4)	2.93	125
C6-H6 ...O1W ¹	3.679(4)	2.84	152
O1W-H12W ...N1 ¹	2.814(3)	2.00(3)	174
O1W-H11W ...N2 ²	2.837(4)	2.01(2)	177
C19-H19 ...O1W ²	3.606(5)	2.75	154
C22-H22 ...O1W ³	3.780(5)	2.92	155
O2-H2A ...O1 ⁴	2.778(4)	1.95(3)	173
(1)-x+2,-y+1,-z	(2)-x+1,-y+1,-z	(3)x-1,+y,+z	(4)x-1,+y,+z+1
Compound (II)			
X-H...Y	X...Y	Y...H	X-H...Y
C6-H6 ...S1	3.133(2)	2.75	106
C2-H2 ...O1 ¹	3.497(2)	2.70	144
C3-H3 ...N1 ²	3.568(2)	2.93	126
O1-H1 ...N1 ²	2.767(2)	1.93(2)	178
C12-H12 ...O1 ³	3.214(3)	2.44	141
(1)-x+1,+y-1/2,-z+1/2+1	(2)-x+1,+y+1/2,-z+1/2+1	(3)-x+1/2+1,-y+2,+z-1/2	

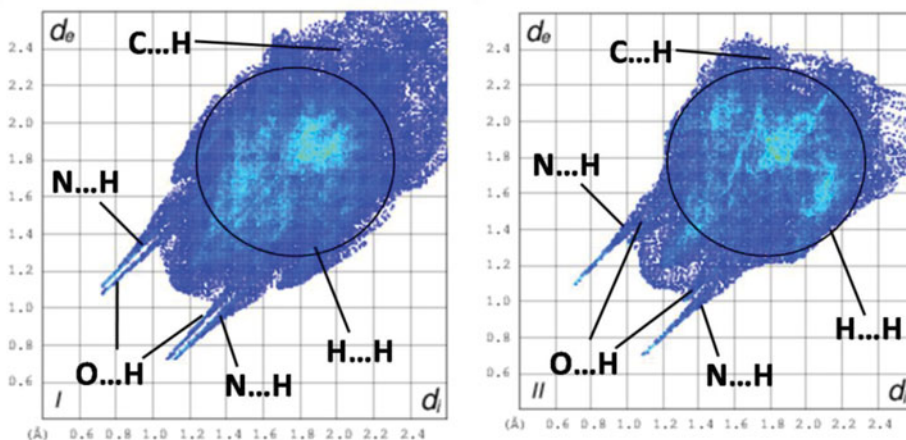


Figure 6. 2D fingerprint plot of compounds (I) and (II), where areas of different intermolecular contacts are clearly shown; d_e and d_i are the distances to the nearest atom centre exterior and interior to the surface.

2.4. Hirshfeld surface calculations

A Hirshfeld surface analysis [27,28] is a technique used to visualize intermolecular interactions and give rise to 3D molecular surface contours. The Hirshfeld surfaces in the crystal structure of particular compound (which may be organic molecule or inorganic metal complex) are constructed on the basis of electron distribution calculated as the sum of electron densities of spherical atom. The 2D fingerprint plots have also been used to examine molecular shapes and give the exact percentage of all important intermolecular contacts which are valuable in the exploration of the packing modes [29]. Distances from points on the surface to a nucleus (atom) inside (d_i) and outside (d_e), the mean surface are determined by the differing vdW radii of atoms, whereby the contact distances d_i and d_e can be normalized (d_{norm}). Therefore, intermolecular interactions (short, moderate, long) in a crystal structure resulting from hydrogen bond donors/acceptors can be visually represented by Hirshfeld surfaces. The value of d_{norm} is -ve or +ve when intermolecular contacts are shorter or longer than van der Waals radii, respectively. The 2-D fingerprint plots summarize the nature and type of intermolecular contacts experienced by the molecules in the crystal. For an each crystal structure,

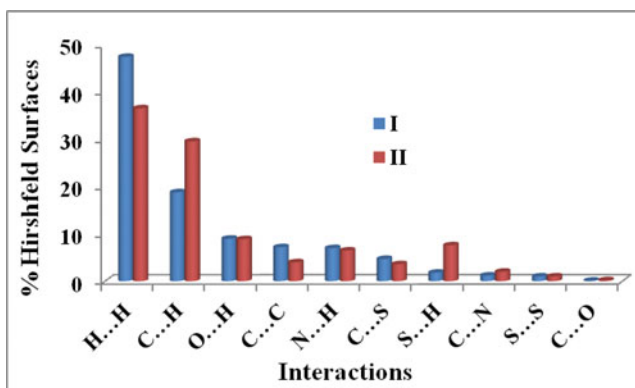


Figure 7. Relative contributions to the Hirshfeld surface area for the various intermolecular contacts (H...H, O...H, C...H, S...H, N...H, C...C, S...S, C...N, C...S and C...O) in compounds (I) and (II).

the Hirshfeld surfaces as well as fingerprint plots are unique, and the number of unique Hirshfeld surfaces depends on the number of crystallographically independent molecules in the corresponding asymmetric unit [30,31].

2.5. Density function theory (DFT) calculations

DFT calculations can be performed by using Gaussian 03 package [32] with 6-31G basis set for all atoms at B3LYP level. These calculations can give rise to the shape of molecular geometries with minimum energies, bond distances (Å), bond angles (°), torsion angles (°) and HOMO-LUMO values etc. The crystal structures of positional isomers are different due to difference in rational design of packing arrangement and intermolecular interactions. Diagrams of molecular orbitals of compounds (I) and (II) are visualized using “gauss view” [33,34].

3. Results and discussion

3.1. Crystal structure of 3-(benzo[d]thiazol-2-yl)phenol (I)

The compound (I) is solved in centrosymmetric triclinic space group $P\bar{1}$. In the molecular structure of this compound two molecules of 3-(benzo[d]thiazol-2-yl)phenol and one lattice water molecule is present (Fig. 1). The packing diagram of complex (I) shows arrangement of molecules within unit cell (Fig. 2a). The dihedral angles between thiol ring and phenyl ring in both molecules of compound (I) are $7.54(10)^\circ$ and $4.33(10)^\circ$. The phenyl ring is twisted from the benzothiazole moiety about the C...C bond, torsion angle C6-C1-C7-S1 is -172.35° , C2-C1-C7-N1 is -172.62° for first molecule and torsion angle C19-C14-C20-S2 is -175.29° , C15-C14-C20-N2 is -175.60° for other molecule of compound (I). The important H-bonding interactions are present between lattice water and molecular unit forming H-bonded tetrahedral geometry as shown in Fig. 3a, along b axis [O1-H1A...O1W = $1.78(3)$ Å, O1W-H12W...N1[#] = $2.00(3)$ Å, O1W-H11W...N2^{#1} = $2.01(2)$ Å, O2-H2A...O1^{#3} = $1.95(3)$ Å, (where [#]: -x+2, -y+1, -z; ^{#1}: -x+1, -y+1, -z; ^{#3}: x-1, +y, +z+1)]. The π - π interactions between phenyl rings, phenyl and thiol rings in ab plane [centroid C1-C6]...centroid (C8-C13) = 3.856 Å, centroid (C7-N1-C8-C13-S1)...centroid (C1-C6) = 3.897 Å] forming extended 1-D chain (Fig. 3b). These are intra and intermolecular interactions and detail of exact percentage of these interactions are explained by Hirshfeld surface analysis.

3.2. Crystal structure of 4-(benzo[d]thiazol-2-yl)phenol (II)

The compound (II) is solved in centrosymmetric orthorhombic space group $Pbca$. In the molecular structure of this compound, only 4-(benzo[d]thiazol-2-yl)phenol is present (Fig. 1). The packing diagram of complex (II) shows arrangement of molecules within unit cell (Fig. 2b). The phenyl ring is not planar with benzothiazole moiety and $18.37(6)^\circ$ dihedral angle is observed between these two rings. The phenyl ring is twisted from the benzothiazole moiety about the C...C bond, torsion angle C2-C1-C7-S1 is 160.16° and C6-C1-C7-N1 is 163.30° . The important H-bonding interactions are observed between proton of hydroxyl (-OH) group and nitrogen atom of pyridyl ring with distance of O1-H1...N1[#] = $1.93(2)$ Å, where [#]: -x+1, +y+1/2, -z+1/2+1. These are intra and intermolecular interactions and detail of these interactions are explained by Hirshfeld surface analysis. A comparison of title structure and those of early reported thiazole derivatives reveal no significant difference observed

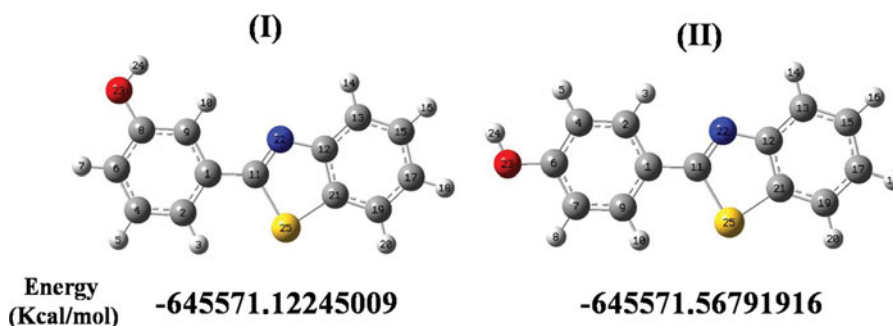


Figure 8. Showing optimized structures of compounds (I) and (II) and their energies after optimization (in Kcal/mol).

either in bond length and bond angles. This compound is already reported in literature [19], but we tried to refine in better way along with weak and strong H-bonded networks reported here. The crystal structure shows H-bonded extended network in *bc* plane through weak CH- π interactions (Fig. 4).

3.3. IR spectroscopy

The experimental result for the C, H, N, S analysis are in good agreement with those calculated for compounds (I) and (II) formed in the reaction. As shown in Figure S1 (SI), the broad band at 3738 cm^{-1} in compound (I) is due to stretching vibrations of -OH group. Weak

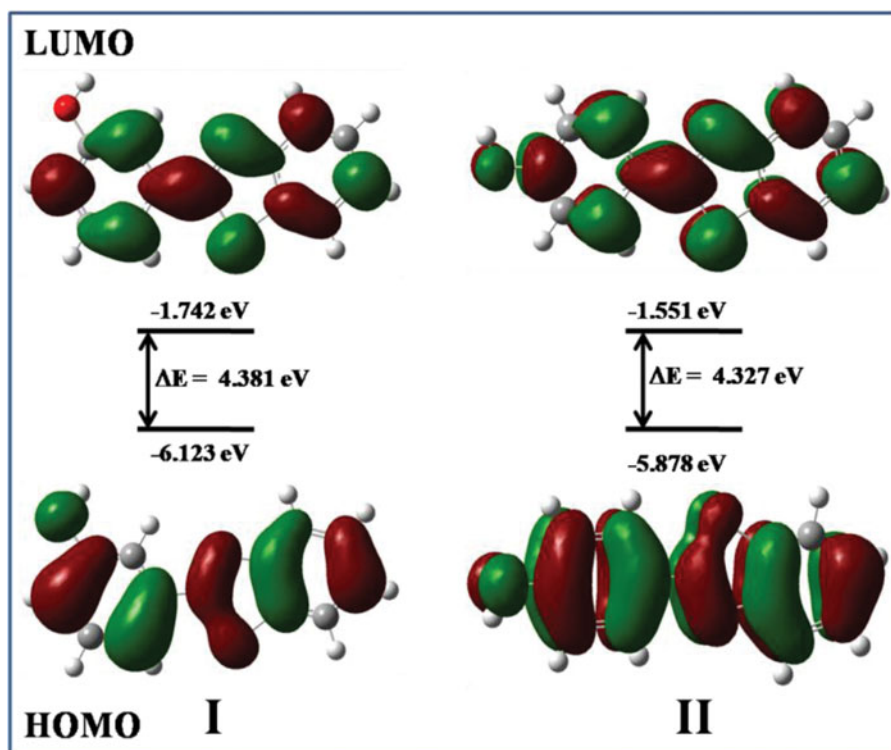


Figure 9. Showing HOMO-LUMO values and energy gap (ΔE value) for compounds (I) and (II).

Table 3. Comparison of selected experimental and calculated geometric parameters (bond lengths (Å), and bond angles (°)) for compound (I).

Compound (I)	Experimental	Theoretical	Deviation
C1-C2	1.3877	1.4056	−0.0179
C1-C6	1.3967	1.4096	−0.0129
C1-C7	1.4719	1.4611	0.0108
C2-C3	1.3733	1.3987	−0.0254
C3-C4	1.3698	1.3952	−0.0254
C4-C5	1.3856	1.4019	−0.0163
C5-C6	1.3867	1.3936	−0.0069
C5-O1	1.355	1.3909	−0.0359
C7-N1	1.3036	1.3004	0.0032
C7-S1	1.7425	1.8688	−0.1263
C8-C9	1.3972	1.403	−0.0058
C8-C13	1.394	1.4169	−0.0229
C8-N1	1.3874	1.3966	−0.0092
C9-C10	1.3623	1.3939	−0.0316
C10-C11	1.3881	1.408	−0.0199
C11-C12	1.3757	1.399	−0.0233
C12-C13	1.4017	1.3947	0.007
C13-S1	1.7299	1.8133	−0.0834
C2-C1-C6	119.5817	119.5095	0.0722
C2-C1-C7	120.9797	122.2598	−1.2801
C6-C1-C7	119.438	118.2306	1.2074
C1-C2-C3	119.5117	119.8521	−0.3404
C2-C3-C4	121.5668	120.8001	0.7667
C3-C4-C5	119.5072	119.2021	0.3051
C4-C5-C6	120.0028	120.7957	−0.7929
C4-C5-O1	118.3742	116.6426	1.7316
C6-C5-O1	121.6229	122.5617	−0.9388
C1-C6-C5	119.8263	119.8405	−0.0142
C1-C7-N1	124.5494	125.1148	−0.5654
C1-C7-S1	120.3827	121.078	−0.6953
N1-C7-S1	115.0659	113.8072	1.2587
C9-C8-C13	119.8374	119.7368	0.1006
C9-C8-N1	125.399	124.7739	0.6251
C13-C8-N1	114.7588	115.4893	−0.7305
C8-C9-C10	118.6623	118.9849	−0.3226
C9-C10-C11	121.646	120.7389	0.9071
C10-C11-C8	121.0587	120.9676	0.0911
C11-C12-C13	117.7144	118.1401	−0.4257
C8-C13-C12	121.0749	121.4316	−0.3567
C8-C13-S1	109.5544	109.9277	−0.3733
C12-C13-S1	129.3666	128.6407	0.7259
C7-N1-C8	111.1919	113.8365	−2.6446
C7-S1-C13	89.4246	86.9394	2.4852

absorption bands at 3045 and 1654 cm^{-1} are due to stretching vibrations of aromatic $-\text{CH}$ and $-\text{C}=\text{N}$ groups respectively. The sharp peaks observed at 1595 cm^{-1} and 793 are due to vibrations in $-\text{C}=\text{C}$ and $-\text{C}-\text{S}$ groups, respectively. In Figure S2 (SI), IR spectrum of compound (II) shows, the broad band at 3657 cm^{-1} is due to stretching vibrations of $-\text{OH}$ group. Weak absorption bands at 2930 and 1620 cm^{-1} are due to stretching vibrations of aromatic $-\text{CH}$ and $-\text{C}=\text{N}$ groups, respectively. The sharp peaks observed at 1576 cm^{-1} and 711 are due to vibrations in $-\text{C}=\text{C}$ and $-\text{C}-\text{S}$ groups respectively. The mass spectra (Figures S3-S4) of the compounds (I) and (II) support their formation. For compound (I), the peak of high intensity is observed at 548.06 corresponds to the molecular ion and two molecules of DMSO (dimethyl sulphoxide) solvent. Another peak at 476.05 corresponds to the molecular ion peak. In mass spectrum of compound (II), the base peak at 227.12 corresponds to the molecular ion peak.

Table 4. Comparison of selected experimental and calculated geometric parameters (Torsion angles (°)) for compound (**I**).

Compound (I)	Experimental	Theoretical	Deviation
C6-C1-C2-C3	0.056	0.0003	0.0557
C7-C1-C2-C3	179.7815	179.9991	−0.2176
C2-C1-C6-C5	0.3809	−0.0002	0.3811
C7-C1-C6-C5	−179.3488	−179.999	0.6502
C2-C1-C7-N1	−172.6204	−179.9639	7.3435
C2-C1-C7-S1	7.9224	0.0442	7.8782
C6-C1-C7-N1	7.1054	0.0349	7.0705
C6-C1-C7-S1	−172.3517	−179.957	7.6053
C1-C2-C3-C4	−0.5515	0.00	−0.5515
C2-C3-C4-C5	0.5965	−0.0005	0.597
C3-C4-C5-C6	−0.1443	0.0006	−0.1449
C3-C4-C5-O1	−179.9556	−179.9995	0.0439
C4-C5-C6-C1	−0.3376	−0.0003	−0.3373
O1-C5-C6-C1	179.5592	179.9998	−0.4406
C1-C7-N1-C8	−179.7799	−179.9942	0.2143
S1-C7-N1-C8	−0.737	−0.0018	−0.7352
C1-C7-S1-C13	−179.9333	−179.9947	0.0614
N1-C7-S1-C13	0.5602	0.0019	0.5583
C13-C8-C9-C10	−0.1154	−0.0006	−0.1148
N1-C8-C9-C10	179.0411	179.9988	−0.9577
C9-C8-C13-C12	−0.2411	0.00	−0.2411
C9-C8-C13-S1	−179.0898	−179.9997	0.9099
N1-C8-C13-C12	−179.484	−179.9995	0.5155
N1-C8-C13-S1	−0.1531	0.0008	−0.1539
C9-C8-N1-C7	−178.6233	−180.0012	1.3779
C13-C8-N1-C7	0.571	0.0006	0.5704
C8-C9-C10-C11	0.7263	0.0005	0.7258
C9-C10-C11-C12	−0.9978	0.0002	−0.998
C10-C11-C12-C13	0.6106	−0.0008	0.6114
C11-C12-C13-C8	−0.0066	0.0007	−0.0073
C11-C12-C13-S1	−179.1909	−180.0003	−0.8094
C8-C13-S1-C7	−0.2053	−0.0014	−0.2039
C12-C13-S1-C7	179.0534	179.999	−0.9456

3.4. Hirshfeld surface calculations

A Hirshfeld surface analysis [27] was performed to visualize the different intermolecular interactions in crystal structures employing 3D molecular surface contours. The Hirshfeld surfaces in the crystal structure of organic compounds are constructed on the basis of calculated electron distribution as the sum of spherical atom electron densities. Some properties can be mapped on Hirshfeld surface: like d_e = the distance from the Hirshfeld surface to the nearest nucleus outside the surface, d_i = the corresponding distance to the nearest nucleus inside the surface, d_{norm} = a normalized contact distance, the sum of these two (d_i and d_e) normalized by the van der Waals radii quantities. Where atoms make intermolecular contacts closer than the sum of their van der Waals radii, these contacts will be highlighted in red on the d_{norm} surface. Longer contacts are blue, and contacts around the sum of van der Waals radii are white [28]. Moreover, 2D fingerprint plots (introduced by Spackman and McKinnon) [29,31] which clearly identify each type of intermolecular interactions produced. They not only indicate which intermolecular interactions are present, but also the relative area of the surface corresponding to each kind of interaction.

The 2D fingerprint plots have also been used to examine molecular shapes and give the exact percentage of all important intermolecular contacts. Many applications in the recent past demonstrated that this analysis can be very valuable in the exploration of the packing modes and intermolecular contacts [28–31]. The Shape index is the measurement of “which

Table 5. Comparison of selected experimental and calculated geometric parameters (bond lengths (Å), and bond angles (°)) for compound (II).

Compound (II)	Experimental	Theoretical	Deviation
C1-C2	1.3911	1.4105	−0.0194
C1-C6	1.3866	1.4096	−0.023
C1-C7	1.4629	1.4569	0.006
C2-C3	1.3785	1.3921	−0.0136
C3-C4	1.3820	1.4025	−0.0205
C4-C5	1.3884	1.4004	−0.012
C5-C6	1.3866	1.3874	−0.0008
C5-O1	1.3502	1.3911	−0.0409
C7-N1	1.2963	1.3007	−0.0044
C7-S1	1.7498	1.8732	−0.1234
C8-C9	1.3807	1.4029	−0.0222
C8-C13	1.3986	1.4171	−0.0185
C8-N1	1.3973	1.3966	0.0007
C9-C10	1.3761	1.3939	−0.0178
C10-C11	1.3836	1.3942	−0.0106
C11-C12	1.3719	1.4077	−0.0358
C12-C13	1.3915	1.3993	−0.0078
C13-S1	1.7328	1.8140	−0.0812
C2-C1-C6	118.0467	118.5574	−0.5107
C2-C1-C7	119.8423	118.9999	0.8424
C6-C1-C7	122.1062	122.4427	−0.3365
C1-C2-C3	119.6031	120.7327	−1.1296
C2-C3-C4	120.8427	120.8001	0.0426
C3-C4-C5	120.4920	119.7708	0.7212
C4-C5-C6	120.0028	120.3172	−0.3144
C4-C5-O1	121.1412	122.8005	−1.6593
C6-C5-O1	123.3107	125.3737	−2.0630
C1-C6-C5	119.3246	119.9846	−0.6600
C1-C7-N1	124.8254	125.1148	−0.2894
C1-C7-S1	120.3152	120.9384	−0.6232
N1-C7-S1	114.8223	113.6879	1.1344
C9-C8-C13	119.8759	119.6868	0.1891
C9-C8-N1	125.9344	124.7402	1.1942
C13-C8-N1	114.1894	115.5730	−1.3836
C8-C9-C10	119.4882	119.1424	0.3458
C9-C10-C11	121.1412	120.7437	0.3975
C10-C11-C8	121.9893	120.9263	1.063
C11-C12-C13	118.1679	118.1696	−0.0017
C8-C13-C12	120.9332	121.4489	−0.5157
C8-C13-S1	109.6222	109.9260	−0.3038
C12-C13-S1	129.442	128.6251	0.8169
C7-N1-C8	111.8035	113.8906	−2.0871
C7-S1-C13	89.5528	86.9225	2.6303

shape”, the red triangles on Shape index represent concave regions indicating atoms of the $\pi \dots \pi$ stacked molecule above them, and the blue triangles represent convex regions indicating the atoms of the molecule inside these surfaces. The Curvedness conveys the similar information as Shape index, which is the measurement of “how much shape”. The 3D d_{norm} surfaces are mapped over a fixed color scale of -0.628 (red) to 1.424 Å (blue), Shape index mapped in the color range of -1.0 to 1.0 Å and Curvedness in the range of -4.0 to 0.4 Å. The 2D fingerprint plots displayed by using the standard $0.58\text{--}2.7$ Å view, with the d_c and d_i distance scales displayed on the graph axes. The two larger red regions on the bottom left and upper left of the d_{norm} surfaces are correspond to the significant O-H \dots O and O-H \dots N type hydrogen bond interactions, which represent the closest intermolecular interactions in compounds (I) and (II). The large flat region delineated by a blue outline on the Curvedness surfaces indicating $\pi \dots \pi$ stacking in compound (I) and CH $\dots \pi$ interactions in compound

Table 6. Comparison of selected experimental and calculated geometric parameters (Torsion angles (°)) for compound (II).

Compound (II)	Experimental	Theoretical	Deviation
C6-C1-C2-C3	− 0.2393	0.0003	− 0.2396
C7-C1-C2-C3	− 179.4593	− 180.0003	− 0.5410
C2-C1-C6-C5	− 17.6872	− 17.9986	0.3114
C7-C1-C6-C5	− 179.4693	0.0001	− 179.469
C2-C1-C7-N1	− 17.5072	0.0063	− 17.5135
C2-C1-C7-S1	− 160.1562	− 179.9944	19.8382
C6-C1-C7-N1	− 163.3054	− 179.9936	16.6882
C6-C1-C7-S1	− 19.0312	0.0057	− 19.0369
C1-C2-C3-C4	1.0307	1.0319	− 0.0012
C2-C3-C4-C5	0.5965	0.8957	− 0.2992
C3-C4-C5-C6	− 0.1443	0.0028	− 0.1471
C3-C4-C5-O1	179.9556	180.0003	− 0.0447
C4-C5-C6-C1	1.0307	0.9845	0.0462
O1-C5-C6-C1	177.504	177.8098	− 0.3058
C1-C7-N1-C8	− 177.8737	− 179.9996	2.1259
S1-C7-N1-C8	0.096	0.0003	0.0957
C1-C7-S1-C13	− 178.4748	− 180.0003	1.5255
N1-C7-S1-C13	− 0.5881	0.0008	− 0.5889
C13-C8-C9-C10	1.3376	− 0.0006	1.3382
N1-C8-C9-C10	− 178.4311	− 180.0003	1.5692
C9-C8-C13-C12	− 1.3728	0.0003	− 1.3731
C9-C8-C13-S1	179.1633	180.0005	− 0.8372
N1-C8-C13-C12	178.422	179.9876	− 1.5656
N1-C8-C13-S1	− 1.042	1.8023	− 2.8443
C9-C8-N1-C7	− 179.5944	− 179.9999	0.4055
C13-C8-N1-C7	0.6254	− 0.0008	0.6262
C8-C9-C10-C11	0.1751	− 179.9995	180.1746
C9-C10-C11-C12	− 1.725	− 0.0004	− 1.7246
C10-C11-C12-C13	1.6684	0.0001	1.6683
C11-C12-C13-C8	− 0.1387	− 0.0001	− 0.1386
C11-C12-C13-S1	179.2075	180.0003	− 0.7928
C8-C13-S1-C7	0.8841	− 0.0016	0.8857
C12-C13-S1-C7	178.5205	179.9986	− 1.4781

(II) (Fig. 5). The 2D fingerprint plot of compound (I) shows sharp spikes of O ...H interactions towards inner side and other sharp spikes of N ...H interactions towards outer side but spikes of O ...H interactions in compound (II) are less prominent. The proportion of intermolecular interactions calculated by 2D fingerprint plot (Fig. 6, Figures S5–S6) were found to be 47.4%, 18.7%, 9.0%, 7.2%, 7.0%, and 4.7% for H-H, C-H, O-H, C-H, N-H, and C-S contacts to the total Hirshfeld surfaces for compound (I) whereas 36.5%, 29.5%, 8.9%, 4.0%, 6.5%, and 3.6% for H-H, C-H, O-H, C-H, N-H, and C-S contacts to the total Hirshfeld surfaces for compound (II) (Fig. 7).

Table 7. Chemical reactivity indices for compounds (I) and (II).

Codes	(I)	(II)
HOMO (eV)	− 6.123	− 5.878
LUMO (eV)	− 1.742	− 1.551
ΔE (eV)	4.381	4.327
μ (eV) [#]	− 3.933	− 3.715
η (eV) ^{##}	2.191	2.164
ω (eV) ^{###}	3.530	3.189

$$^{\#} \mu = (E_{\text{HOMO}} + E_{\text{LUMO}}) / 2, ^{##} \eta = (E_{\text{LUMO}} - E_{\text{HOMO}}) / 2, ^{###} \omega = \mu^2 / 2\eta.$$

3.5. DFT calculations

A density functional theory (DFT) geometry calculation have been done with GAUSSIAN-03 program package employing the B3LYP (Becke three parameter Lee-Yang-Parr) exchange correlation functional and the 6-31 G(d) basis set was performed [33,34] on compounds (I) and (II). Diagram of molecular orbital is visualized using “gauss view” [34]. No solvent corrections were made with these calculations. Starting geometries were taken from X-ray refinement data. The optimized geometric results in the free molecule state are, therefore, compared to those in the crystalline state and energies after optimization (in Kcal/mol) of both compounds are also shown in Fig. 8. In addition, a comparison of strong and weak intermolecular hydrogen bond interactions have been included in a discussion of the structural aspects. Optimized structure of compounds (I) and (II) were compared with those obtained from X-ray diffraction analysis studies. In both cases, the bond distances (Å) and angles (°) of optimized (theoretical) data are similar to the structural (experimental) data and there is negligible deviation in them but there are significant differences in the torsion angles (Tables 3–6). The HOMO-LUMO values and their energy gaps (ΔE) of compounds (I) and (II) are given in Fig. 9.

In the compound (I), the highest occupied molecular orbital (HOMO) is localized over the smaller regions of phenyl and thiazolyl rings and oxygen atom of $-OH$ group whereas lowest unoccupied molecular orbital (LUMO) is most distributed mainly over the nitrogen, sulfur atoms and some carbon atoms of aromatic rings except the $-OH$ group.

In the compound (II), the HOMO is localized all over the molecule including $-OH$ group whereas LUMO is most distributed mainly over small regions of the nitrogen, sulfur atoms, some carbon atoms of aromatic rings and oxygen of $-OH$ group. Larger the HOMO-LUMO energy gap, more stable and less reactive molecule is formed. ΔE value of (I) is 4.381 eV and compound (II) is 4.327 eV, so (I) is more stable and less reactive than (II). On the basis of molecular orbitals, the values of chemical hardness (η), electronic chemical potential (μ), global electrophilicity index (ω) etc. of compounds can be calculated [35,36]. Global electrophilicity index (ω), introduced by Parr [37], and measures the propensity or capacity of a species to accept electrons. Chemical reactivity indices for compounds (I) and (II) are given in Table 7 which shows that chemical hardness of compound (I) is comparatively high than (II). The results of μ , though are not so conclusive for (I) and (II). Compound (I) is nucleophilic and presence of lattice or coordinated water molecules (in aqueous medium) increases nucleophilicity of particular compound.

4. Conclusion

The compounds (I) and (II) have been crystallized in centrosymmetric triclinic and orthorhombic space groups respectively. These two positional isomers are differ in packing arrangement in unit cell, inter and intramolecular H-bonding interactions. The DFT optimized molecular geometries in compounds (I) and (II) agree closely with those obtained from the crystallographic studies. The HOMO-LUMO gap in (I) is higher than (II) which indicate the greater stability, hardness and lesser reactivity of (I) as compare to (II). The melting point of (I) is higher than (II) because of lattice water leads to stability by strong H-bonding interactions and increases the nucleophilicity of this compound in aqueous medium which is also confirmed by DFT calculations. An interplay of $O-H \dots O_w$ and $O-H \dots N$ type strong hydrogen bonds and $C-H \dots S$ type weak interactions connect the molecules of (I) and (II) into 2D framework. Hirshfeld surface analysis of (I) indicate that the $H \dots H$ and $H \dots \pi$ contacts can

account for 47.4% and 18.7%, respectively, of the total Hirshfeld surface area, whereas the corresponding fraction in (II) is 36.5% and 29.5%, respectively.

Acknowledgements

RK Mudsainiyan gratefully acknowledges UGC-BSR for financial assistance. AK Jassal thanks DST for INSPIRE fellowship.

References

- [1] Chen, K.-Y., Fang, T.-C., Chang, M.-J., Tsai, H.-Y., & Luo, M.-H. (2011). *Acta Cryst.*, E67, o2862.
- [2] Yousuf, S., Shah, S., Ambreen, N., Khan, K. M., & Ahmed, S. (2012). *Acta Cryst.*, E68 o2799.
- [3] Yousuf, S., Shah, S., Ambreen, N., Khan, K. M., Ahmad, S. (2012). *Acta Cryst.*, E68, o3057.
- [4] Yousuf, S., Shah, S., Ambreen, N., Khan, K. M., & Ahmad, S. (2012). *Acta Cryst.*, E68, o2877.
- [5] Zhang, Y., Qu, Y., Zhao, B. I. (2010). *Acta Cryst.*, E66, o2143.
- [6] Vijayakumar, S., Murugavel, S., Selvakumar, R., & Bakthadoss, M. (2012). *Acta Cryst.*, E68, o2362.
- [7] Lakshmanan, D., Raj, R. M., Selvakumar, R., Bakthadoss, M., & Murugavel, S. (2011). *Acta Cryst.*, E67, o2259.
- [8] Zhang, Y., Su, Z.-H., Wang, Q.-Z., & Teng, L. (2008). *Acta Cryst.*, E64, o2065.
- [9] Angelopoulos, N., Hadjiprocopis, A., & Walkinshaw, M. D. (2009). *J. Chem. Inf. Model.*, 49, 1547.
- [10] Sankaran, M., Kumarasamy, C., Chokkalingam, U., Mohan, P. S. (2010). *Bioorg. Med. Chem. Lett.*, 20, 7147.
- [11] Zhang, X., Shetty, A. S., & Jenekhe, S. A. (1999). *Macromolecules*, 32, 7422.
- [12] Pearce, D. A., Jotterand, N., Carrico, I. S., & Imperiali, B. J. (2001). *Am. Chem. Soc.*, 123, 5160.
- [13] Sameiro, M., & Gonçalves, T. (2009). *Chem. Rev.*, 109, 190.
- [14] Arriaga, E. A., Zhang, Y., & Dovichi, N. J. (1995). *Ana. Chim. Acta*, 299, 319.
- [15] Jiang, P., & Guo, Z. (2004). *Coord. Chem. Rev.*, 248, 205.
- [16] Weng, J. Q., Liu, X. H., Huang, H., & Tan, C. X. (2012). *J. Chem. Molecules*, 17, 989.
- [17] Bakavoli, M., Rahimizadeh, M., Feizyadeh, B., Kaju, A. A., & Takjoo, R. (2010). *J. Chem. Crystallogr.*, 40, 746.
- [18] González-Rodríguez, D., & Schenning, A. P. H. J. (2011). *Chem. Mater.*, 23 310.
- [19] Teo, S.-B., Okechuckwu, R. C., & Teoh, S.-G. (1995). *Acta Cryst.*, C51, 1629.
- [20] Allen, F.H. (2002). *Acta Cryst.*, B58, 380.
- [21] Altomare, A., Cascarano, G., Giacovazzo, C., & Guagliardi, A. (1993). *J. Appl. Crystallogr.*, 26, 343.
- [22] Sheldrick, G. M. (2008). *Acta Cryst.*, A64 112.
- [23] Nardelli, M. (1983). *Comput. Chem.*, 7 95.
- [24] Farrugia, L. J. (1997). *J. Appl. Crystallogr.*, 30, 565.
- [25] Allen, F. H. (2002). *Acta Cryst.*, B58, 380.
- [26] Farrugia, L. J., (1999). *J. Appl. Cryst.*, 32, 837.
- [27] McKinnon, J. J., Jayatilaka, D., & Spackman, M. A. (2007). *Chem. Commun.*, 1.
- [28] Li, Y., Zhang, C. G., Cai, L. Y., Wang, Z. X. (2013). *J. Coord. Chem.*, 66, 3100.
- [29] McKinnon, J. J., Spackman, M. A., & Mitchell, A. S. (2004). *Acta Crystallogr. Sec. B*, 60, 627.
- [30] McKinnon, J. J., Jayatilaka, D., Spackman, M. A. (2007). *Chem. Commun.*, 37, 3814–3816.
- [31] Spackman, M. A., McKinnon, J. J. (2002). *Cryst. Eng. Comm.*, 4, 378–392.
- [32] Frisch, M.J. et al. (2004). Gaussian 03, Gaussian, Inc., Wallingford CT.
- [33] Becke, A. D. (1993). *J. Chem. Phys.*, 98, 5648–5652.
- [34] Lee, C., Yang, W., Parr, R. G. (1988). *Phys. Rev. B*, 37, 785–789.
- [35] Liu, S. J. (2005). *Chem. Sci.*, 117, 477–483.
- [36] Elango, M. et al. (2005). *Chem. Sci.*, 117, 61–65.
- [37] Parr, R. G., von Szentpaly, L., & Liu, S. J. (1999). *Am. Chem. Soc.*, 121, 1922–1924.